Journal of Power Sources 219 (2012) 199–203

Contents lists available at SciVerse ScienceDirect

Journal of Power Sources

journal homepage: www.elsevier.com/locate/jpowsour

Facile synthesis of SnO_2 nanocrystals coated conducting polymer nanowires for enhanced lithium storage

Zhijia Du, Shichao Zhang*, Tao Jiang, Xiaomeng Wu, Lan Zhang, Hua Fang

School of Materials Science and Engineering, Beihang University, Beijing 100191, PR China

HIGHLIGHTS

- SnO_2 nanoparticles coated polypyrrole nanowires are introduced into Li-ion battery.
- The polypyrrole networks serve as structural support and allow electrolyte immersion.
- The nanostructured composites deliver high capacity and long cycle life.

ARTICLE INFO

Article history:
Received 16 May 2012
Received in revised form
3 July 2012
Accepted 16 July 2012
Available online 23 July 2012

Keywords:
Lithium ion battery
Conducting polymers
Nanowires
SnO_2 nanoparticles

ABSTRACT

SnO_2 nanoparticles uniformly decorated polypyrrole (PPy) nanowires are synthesized by a facile two-step electrochemical reaction method: electropolymerization and electrodeposition. The nanostructured SnO_2–PPy hybrids show porous reticular morphology and homogenous distributions. The reticular SnO_2–PPy nanowires can increase the electrode/electrolyte interface and accommodate the volume variation of SnO_2. When applied as anode materials for lithium ion batteries, the unique nanostructured hybrids deliver meaningfully improved Li^+ storage performance with the first reversible capacity of 690 mAh g^{-1}. This facile synthesis procedure can also be simply grafted to other inorganic–organic hybrid composites.

1. Introduction

One-dimensional nanostructures are of great potential as key functional components for the next generation nanodevices due to their unique and fascinating properties compared to their bulk counterparts [1–3]. It is now recognized that the distinctly improved properties of nanoscale materials probably derives from their enlarged surface areas and quantum confinement effects. SnO_2, as one of the most important semiconductive materials, has attracted extensive efforts for various applications in field effect transistors [4,5], solar cells [6,7], gas sensors [8–10], and catalyst supports [11]. Particularly, SnO_2 is a promising anode candidate in lithium ion batteries owing to its theoretical capacity of 782 mAh g^{-1} which is superior to the currently commercialized graphite (372 mAh g^{-1}) [12,13]. However, previous research demonstrated that SnO_2 suffers from the enormous volume expansion (up to 250% or larger) during lithiation process [14], which leads to severe structural and electronic deterioration, resulting in fierce capacity decay.

Pure SnO_2 nanostructures had been prepared by a variety of procedures to solve this puzzle, including solvothermal process [15,16], electrodeposition [17], engaged coordinating etching [18], and so on. However, in spite of the improved performance, some disadvantages also emerged in their application. For instance, the SnO_2 nanostructures suffered from aggregation during cycling which probably hindered the efficiency of the declared advantage [19,20].

To further improve the above-mentioned properties of nanostructured SnO_2, diverse routes have been developed to design specific configuration of composites with homogenous dispersion of SnO_2 nanostructures into a matrix support such as carbon nanotubes (CNTs), [21–24] graphite particles, [25] and graphene sheets. [26]. The concept of using nanostructured SnO_2 composites is that the volume variation drawback can be efficiently addressed without the aggregation trouble considering that all the SnO_2 nanostructures are individually attached to the structural support.

Previous reports about the integration of SnO_2 with PPy have shown some improvement in the first 20 cycles as anode materials

* Corresponding author. Tel.: +86 10 82338148; fax: +86 01 82339319.
E-mail address: csc@buaa.edu.cn (S. Zhang).

0378-7753/$ – see front matter © 2012 Elsevier B.V. All rights reserved.
http://dx.doi.org/10.1016/j.jpowsour.2012.07.052

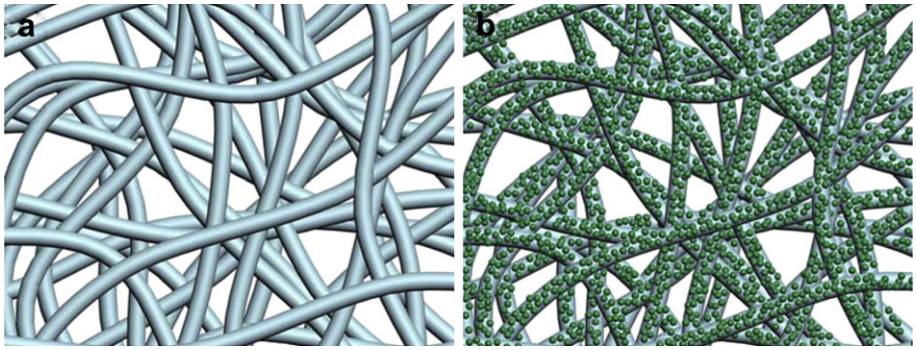

Fig. 1. (a) and (b) The schematic illustration of reticular PPy nanowires before and after SnO_2 nanocrystals deposition.

for lithium ion battery [27,28]. However, it is anticipated that further improvement may be obtained with more well-designed SnO_2–PPy nanostructures. Herein, we introduce a facile strategy to rationally synthesize the hybrid design of specific configuration with homogenous dispersion of SnO_2 nanocrystals into PPy matrix support. Fig. 1a and b illustrate the preparation scheme of the PPy nanowires and the nanostructured SnO_2–PPy hybrids. The PPy nanowires networks are employed as backbones of the three-dimensional (3D) microstructure. The SnO_2 nanocrystals are contrived to uniformly dispersing on the surface of the 3D PPy backbones. As an application for lithium ion batteries, the novel nanostructured hybrids deliver meaningfully improved Li storage performance, with a reversible capacity of 622 mAh g^{-1} retained after 80 cycles.

2. Experimental

The 3D reticular PPy nanowires were synthesized by electropolymerization from the pyrrole monomer solution. The solution consisted of 0.3 M $KClO_4$ and 0.5 M pyrrole. Nickel foil, Pt foil and saturated calomel electrode (SCE) were used as the working, counter and reference electrode, respectively. The electropolymerization was carried out under 0.7 V for 200 s at 35 °C. Then the PPy nanowires were rinsed with distilled water and dried at 80 °C for 20 h in vacuum. Subsequently, tin dioxide was electrodeposited on the PPy nanowires in an aqueous solution consisting of 10 mM $SnCl_2$ and 50 mM HNO_3. Oxygen is blown into the mixed solutions at a bath temperature of 85 °C for 1 h to oxidize the stannous ions into the stannic ions. Electrodeposition was conducted under 0.8 mA cm^{-2} for 30 min. The mass of the PPy nanowires and SnO_2 coating were calculated by measuring the Ni foil each time before and after the PPy electropolymerization and SnO_2 electrodeposition *via* a METTLER AB135-S analytical balance. The amount proportion of SnO_2 (wt.%) was about 78% in the PPy–Si nanocomposites. For convenience, the calculation of the capacity is based solely on SnO_2.

The morphology was characterized by a field emission scanning electron microscopy (FE-SEM, Hitachi S-4800) and a field emission transmission electron microscope (FE-TEM, JEM-2100F). Powder X-ray diffraction (XRD) patterns were obtained on a Rigaku D/MAX 2000 PC diffractometer operating at 40 kV and 25 mA, using Cu Ka radiation ($\lambda = 1.5406$Å).

Half-cells were assembled with the composite, lithium foil and Celgard 2300 membrane in an Ar-filled glove box (MB-10-G, MBRAUN). The electrolyte was 1 M $LiPF_6$ in a 50:50 (v/v) mixture of ethylene carbonate (EC) and diethyl carbonate (DEC). The galvanostatic measurements were carried out in a battery test system (Arbin electrochemical instrument).

3. Results and discussion

3.1. The synthesis of PPy nanowires on Ni foil

Fig. 2a displays the synthetic scheme of the PPy nanowires. The PPy reticular nanowires are prepared by electropolymerization of the pyrrole monomers from their solution, in which the electrode potential functions as the driving force for the initiation and further polymerization. The first step is the transfer of the electron from the pyrrole monomers to the electrode, which results in the formation of cationic radicals. Dimers are subsequently formed by addition dimerization and removal of two protons. The dimers were reoxidized and repolymerized to the long chain PPy.

The chain propagation of PPy nanowires with the elapsed time is well elucidated in Fig. 2b, c and d. The length of the PPy

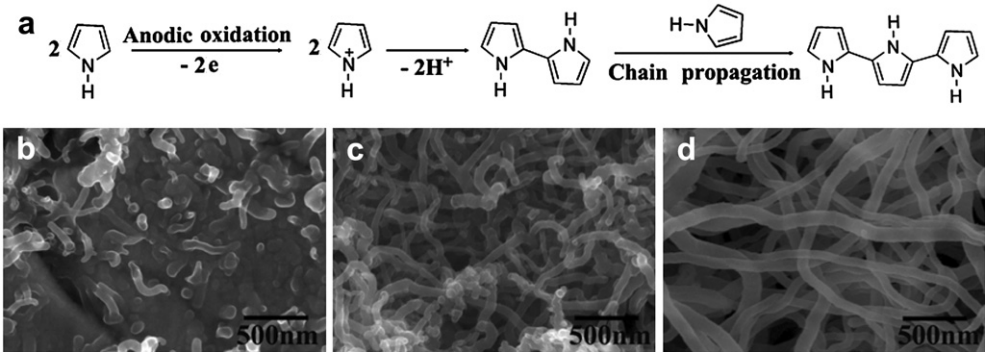

Fig. 2. (a) Scheme of the electropolymerization procedure of PPy. (b), (c) and (d) The SEM images of PPy nanowires after electropolymerization for 10 s, 90 s and 200 s, respectively.

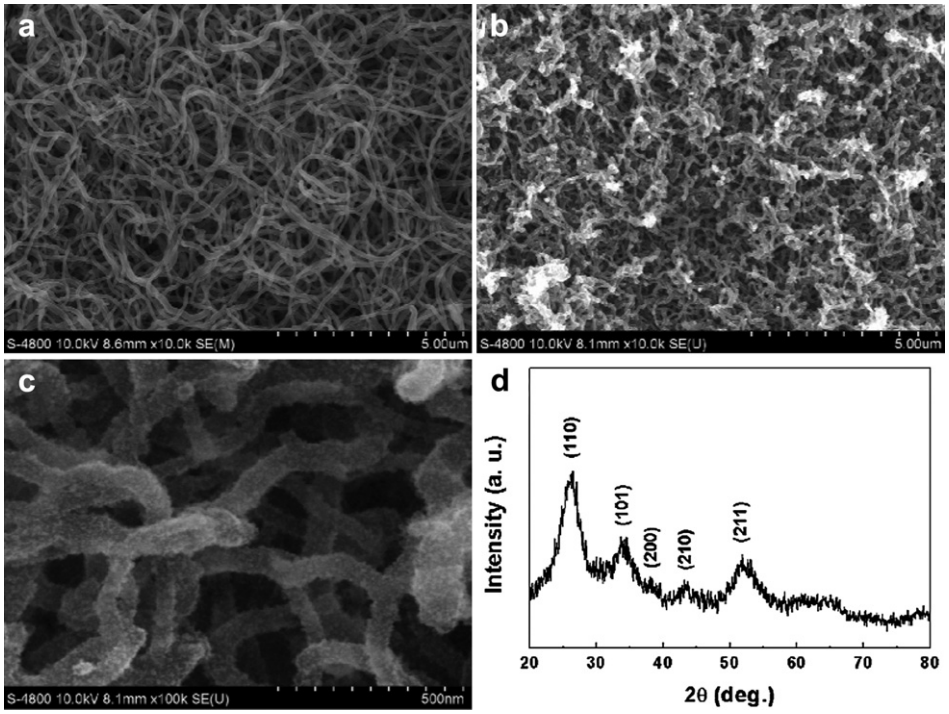

Fig. 3. (a) SEM image of the PPy nanowires for 200 s. (b) and (c) Low and high magnification SEM images of the SnO_2–PPy hybrid after 30 min deposition, respectively. (d) XRD patterns of the electrodeposited SnO_2 nanocrystals.

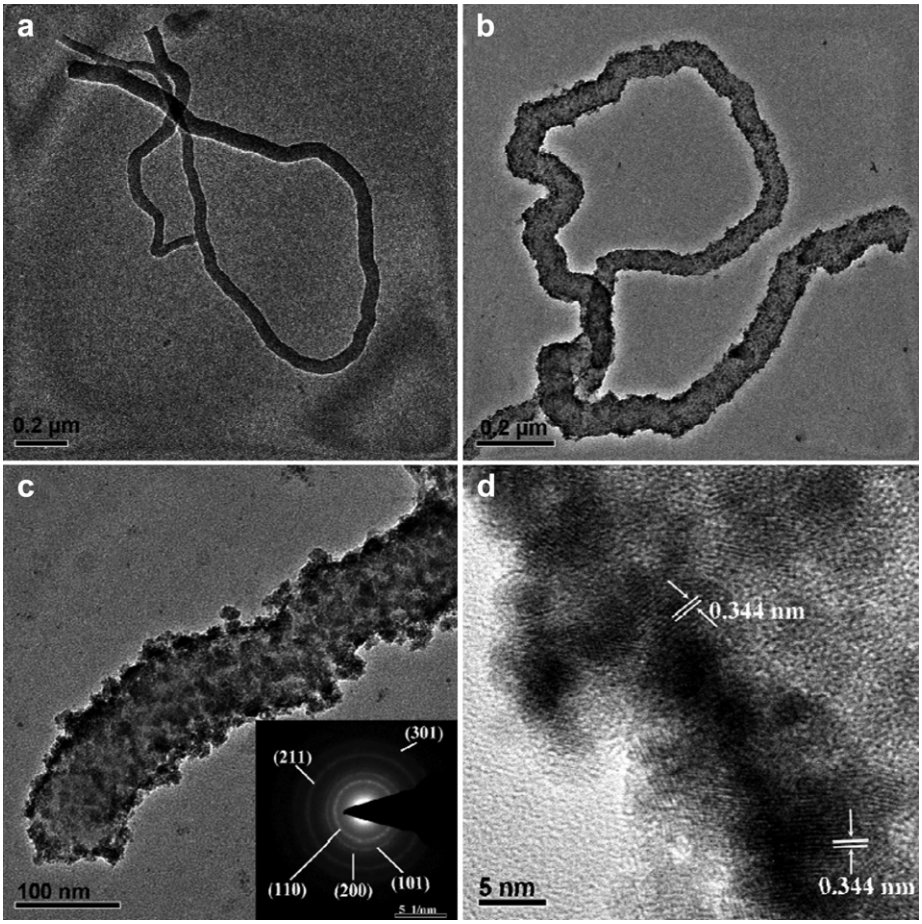

Fig. 4. (a) TEM image of the as-prepared PPy nanowires. (b) and (c) Low and high magnification TEM images of the SnO_2–PPy hybrid, respectively. The inset of (c) is the SAED image of the electrodeposited SnO_2. (d) HRTEM image revealing nanocrystal SnO_2 particles attached to the PPy nanowires.

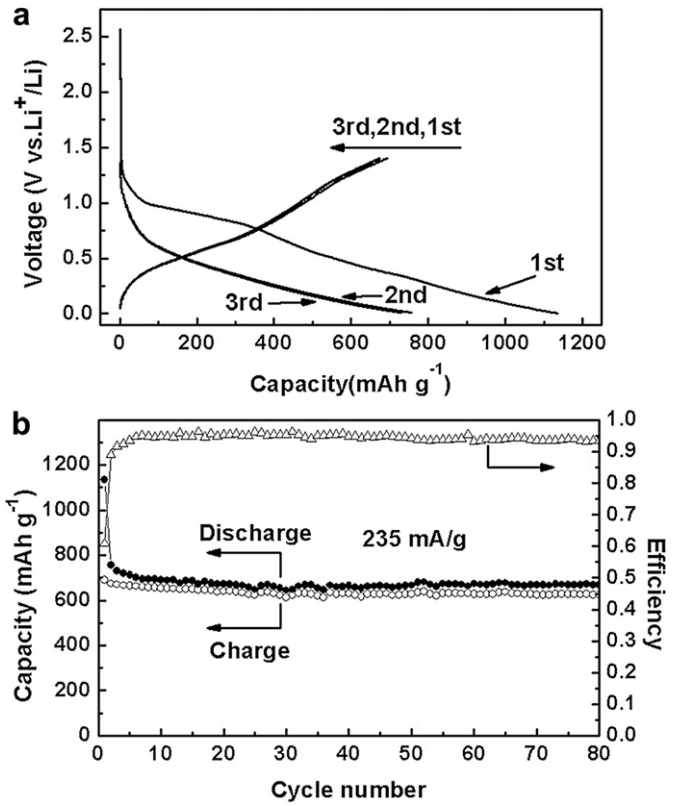

Fig. 5. (a) Voltage profiles of the nanostructured composite in half cells cycled between 5 mV and 1.4 V at a rate of 0.3 C (=235 mA g^{-1}). (b) The cycling performance of the half cell at 0.3 C.

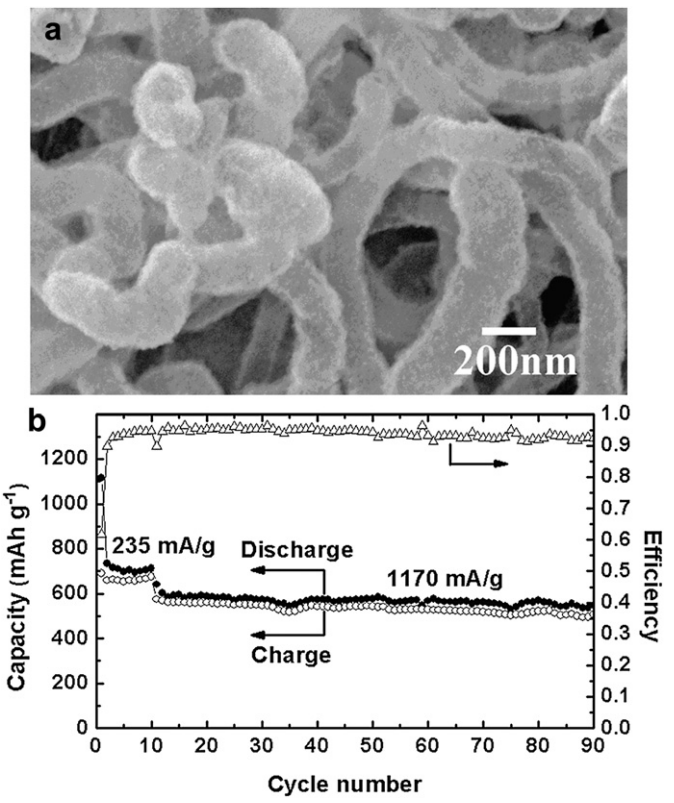

Fig. 6. (a) SEM image of the nanostructured SnO_2–PPy composite after 80 cycles at 0.3 C. (b) The cycling performance of the half cell at 1.5 C after operating 10 cycles at 0.3 C.

nanowires is tens of nanometers for 10 s, and increases to several micrometers for 200 s. The morphology of the reticular PPy nanowires polymerized for 200 s is shown in Fig. 3a, revealing an interlaced network microstructure. The diameter of these nanowires is 70–120 nm.

3.2. The synthesis and characterization of SnO_2–PPy nanocomposites

The PPy reticular nanowires are subsequently applied as the substrate for the deposition of SnO_2 nanocrystals *via* an electrochemical conversion reaction [29]:

$$NO_3^- + H_2O + 2e^- \rightarrow NO_2^- + 2OH^- \quad (1)$$

$$Sn^{4+} + 4OH^- \rightarrow Sn(OH)_4 \rightarrow SnO_2 + H_2O \quad (2)$$

Electrodeposition of SnO_2 nanocrystals is carried out for 30 min. The 3D nanostructured SnO_2–PPy composites inherit the reticular morphology to a great extent as presented in Fig. 3b. The evolution of smooth surface for PPy nanowires into the rough surface for the composites indicates that the PPy nanowires are all cover with SnO_2, which is further confirmed in the high-magnification SEM image in Fig. 3c. It can be seen that particulate deposits are densely packed on the surface of PPy nanowires. The average size of the particles is several nanometers. X-ray diffraction (XRD) is conducted to confirm the phase of the deposited SnO_2 in Fig. 3d. All of the reflection peaks can be indexed to the tetragonal rutile-like tin dioxide phase referring to JCPDS No. 41-1445.

Transmission Electron Microscope (TEM) is carried out to further investigate the inherent nanostructure of the SnO_2–PPy hybrids as exhibited in Fig. 4. The maximum length of the PPy nanowires (Fig. 4a) can reach several micrometers. Fig. 4b and c distinctly reveal that the surface of PPy nanowires is thoroughly coated with particulate SnO_2 after 30 min electrodeposition. The corresponding selected area electron diffraction (SAED) pattern (inset in Fig. 4c) can be indexed as (110), (101), (200), (211), and (301) planes of rutile type SnO_2 (JCPDS No. 41-1445). The ring-like SAED pattern reveals the overall polycrystallinity of the SnO_2 structure. The diffraction lattice planes in high-resolution TEM image (Fig. 4d) indicates that the SnO_2 particles are well crystallized. The size of individual grains is most likely less than 10 nm in both dimensions.

3.3. The CV and charge/discharge profile of SnO_2–PPy anode

PPy alone was previous investigated by cyclic voltammogram (CV) swept from 1.6 V to 0.01 V (vs. Li^+/Li) where the current obtained was insignificant [30]. The result distinctly demonstrated that PPy had no electrochemical activity toward lithium insertion in this potential range. After the construction of our well-designed inorganic–organic nanostructure, the PPy nanowires serve as the 3D structural support while the particulate SnO_2 functions as the Li storage component.

Fig. 5a depicts the charge/discharge profile of the SnO_2–PPy nanocomposite at current density of 235 mA g^{-1} and a voltage cutoff of 1.4/0.005 V for the first three cycles. Generally, the electrochemical reaction of SnO_2 with lithium can be explained as the following two equations: $SnO_2 + 4Li^+ + 4e^- \rightarrow Sn + 2Li_2O$ (a); $Sn + xLi^+ + xe^- \leftrightarrow Li_xSn$ (b). Reaction (a) is generally regarded irreversible, thus, the theoretical capacity of SnO_2 is determined as 782 mAh g^{-1} by the reversible reaction (b). In the first discharge,

there is a substantial plateau at around 0.9 V, which disappears in the following cycles. This irreversible plateau is assigned to the formation of solid electrolyte interface (SEI) layer and the reduction of SnO_2 into Li_2O and zero-valent Sn [12,31]. Afterward, the voltage decreases continuously to 5 mV. This sloping region is related to the lithium alloying process with Sn to form constitutive Li_xSn alloys as described in reaction (b). After the first discharge, the electrochemical reaction can be considered as reversible lithiation/delithiation process between lithium and tin nanocrystals. The profiles of the 2nd and 3rd cycles overlap very well, implying a stead Li insertion/extraction mechanism into/from the nanostructured composite.

3.4. The cycling performance of SnO_2–PPy anode

Fig. 5b shows the cycling performance of the nanostructured SnO_2–PPy composites at 0.3 C rate. The first discharge and charge capacities are 1134 and 690 mAh g^{-1}, respectively, giving an initial Coulombic efficiency of 61%. The irreversible capacity can be attributed to the trapped Li^+ in forms of Li_2O and the SEI formation due to the decomposition of electrolyte as discussed above. The discharge and charge capacities maintain well from the 2nd cycle onwards. For example, the reversible capacity at the 80th cycle is 622 mAh g^{-1}, providing a relatively high retention rate of 90%. This capacity retaining capability is highly superior to the nanostructured SnO_2 electrode, such as hollow nanoboxes and nanosheets [18,32]. Moreover, it is comparable to or fairly higher than the recent reports about the nanostructured SnO_2–C composites, such as SnO_2 nanorod-planted graphite [25], SnO_2 coated carbon nanotubes (CNTs) [22], and CNTs@SnO_2@C coaxial nanocables [21]. However, our two-step electrochemical reaction strategy is more economical and facile to realize. The improvement in electrochemical performance should be ascribed to the configuration of the nanostructured SnO_2–PPy composites which offers three distinct advantages. Firstly, the 3D reticular PPy nanowires function as the structural support and allow the convenient gathering and delivering for Li^+ and electron. Secondly, the nanoscale SnO_2 particles are favorable for volume accommodation which thereby results in the impressive cycling stability. Finnally, the 3D porous nature of the nanocomposites is capable of complete penetration of electrolyte which improves the electrochemical reaction dynamics.

Fig. 6a displays the SEM image of the nanostructured composites after 80 cycles. Apparently, the morphology shows less variation but ambiguous boundaries between adjacent SnO_2 particles and the thickening of the nanowires. This may be induced by two reasons: one is the SEI formation on the electrode surface; the other is that the SnO_2 particles may joint them with each other due to the volume expansion during Li^+ insertion. Overall, the microstructure of SnO_2–PPy composite retains after repeat charge/discharge process due to the above mentioned profit. Additionally, the remarkable cycling durability of the electrode at 1.5 C rate is also tested and demonstrated in Fig. 6b. The capacities at the 11th and 90th cycle are 576 and 506 mAh g^{-1}, respectively, with appealing retention rate of 88%.

4. Conclusions

In summary, we report a facile two-step process, electropolymerization and electrodeposition, to fabricate the nanostructured SnO_2–PPy composites as anode materials for lithium ion batteries. SEM and TEM reveal that the surface of PPy nanowires is densely coated with nanoscale SnO_2 particles. The novel inorganic-organic nanocomposites are competent for high performance anode materials. The electrode delivers a high and stable reversible capacity above 600 mAh g^{-1} for 80 cycles at 0.3 C. We believe that this specific designed configuration may be also attractive for other applications such as solar cells, gas sensor, and electrochemical capacitors.

Acknowledgments

This work was supported by the National Natural Science Foundation of China (50954005, 51074011), National Basic Research Program of China (2007CB936502), National 863 Program (2006AA03Z230 and 2008AA03Z208), and the Scholarship Award for Excellent Doctoral Student granted by China Ministry of Education.

Appendix A. Supplementary material

Supplementary data associated with this article can be found, in the online version, at http://dx.doi.org/10.1016/j.jpowsour.2012.07.052.

References

[1] Y. Xia, P. Yang, Y. Sun, Y. Wu, B. Mayers, B. Gates, Y. Yin, F. Kim, H. Yan, Adv. Mater. 15 (2003) 353.
[2] C.M. Lieber, Z.L. Wang, MRS Bull. 32 (2007) 99.
[3] H.-W. Liang, S. Liu, S.-H. Yu, Adv. Mater. 22 (2010) 3925.
[4] S.H. Lee, G. Jo, W. Park, S. Lee, Y.-S. Kim, B.K. Cho, T. Lee, W.B. Kim, ACS Nano 4 (2010) 1829.
[5] E.J. Boyd, S.A. Brown, Nanotechnology 20 (2009) 425201.
[6] M.A. Hossain, J.R. Jennings, Z.Y. Koh, Q. Wang, ACS Nano 5 (2011) 3172.
[7] H.J. Snaith, C. Ducati, Nano Lett. 10 (2010) 1259.
[8] J.M. Baik, M. Zielke, M.H. Kim, K.L. Turner, A.M. Wodtke, M. Moskovits, ACS Nano 4 (2010) 3117.
[9] Y. Wang, X. Jiang, Y. Xia, J. Am. Chem. Soc. 125 (2003) 16176.
[10] Q. Kuang, C. Lao, Z.L. Wang, Z. Xie, L. Zheng, J. Am. Chem. Soc. 129 (2007) 6070.
[11] M. Niu, F. Huang, L. Cui, P. Huang, Y. Yu, Y. Wang, ACS Nano 4 (2010) 681.
[12] I.A. Courtney, J.R. Dahn, J. Electrochem. Soc. 144 (1997) 2045.
[13] I.A. Courtney, R.A. Dunlap, J.R. Dahn, Electrochim. Acta 45 (1999) 51.
[14] M.-S. Park, G.-X. Wang, Y.-M. Kang, D. Wexler, S.-X. Dou, H.-K. Liu, Angew. Chem. Int. Ed. 46 (2007) 750.
[15] J. Ye, H. Zhang, R. Yang, X. Li, L. Qi, Small 6 (2010) 296.
[16] J. Liu, Y. Li, X. Huang, R. Ding, Y. Hu, J. Jiang, L. Liao, J. Mater. Chem. 19 (2009) 1859.
[17] S.-L. Chou, J.-Z. Wang, H.-K. Liu, S.-X. Dou, Electrochem. Commun. 11 (2009) 242.
[18] Z. Wang, D. Luan, F.Y.C. Boey, X.W. Lou, J. Am. Chem. Soc. 133 (2011) 4738.
[19] Y. Wang, J.Y. Lee, B.H. Chen, Electrochem. Solid-State Lett. 6 (2003) A19.
[20] Y. Li, B. Tan, Y. Wu, Nano Lett. 8 (2008) 265.
[21] P. Wu, N. Du, H. Zhang, J. Yu, D. Yang, J. Phys. Chem. C 114 (2010) 22535.
[22] J. Ren, J. Yang, A. Abouimrane, D. Wang, K. Amine, J. Power Sources 196 (2011) 8701.
[23] G. Chen, Z. Wang, D. Xia, Chem. Mater. 20 (2008) 6951.
[24] Z. Wen, Q. Wang, Q. Zhang, J. Li, Adv. Funct. Mater. 17 (2007) 2772.
[25] J.G. Kim, S.H. Nam, S.H. Lee, S.M. Choi, W.B. Kim, ACS Appl. Mater. Interfaces 3 (2011) 828.
[26] Y. Li, X. Lv, J. Lu, J. Li, J. Phys. Chem. C 114 (2010) 21770.
[27] L. Yuan, J. Wang, S.Y. Chew, J. Chen, Z.P. Guo, L. Zhao, K. Konstantinov, H.K. Liu, J. Power Sources 174 (2007) 1183.
[28] L. Cui, J. Shen, F. Cheng, Z. Tao, J. Chen, J. Power Sources 196 (2011) 2195.
[29] S.T. Chang, I.C. Leu, M.H. Hon, J. Cryst. Growth 273 (2004) 195.
[30] B. Veeraraghavan, J. Paul, B. Haran, B. Popov, J. Power Sources 109 (2002) 377.
[31] C.-M. Wang, W. Xu, J. Liu, J.-G. Zhang, L.V. Saraf, B.W. Arey, D. Choi, Z.-G. Yang, J. Xiao, S. Thevuthasan, D.R. Baer, Nano Lett. 11 (2011) 1874.
[32] C. Wang, Y. Zhou, M. Ge, X. Xu, Z. Zhang, J.Z. Jiang, J. Am. Chem. Soc. 132 (2010) 46.